

The origin of the mediocre methanol selectivity of Cu/ZnO-based catalysts for methanol synthesis from CO₂ hydrogenation

Ziyang Chen ^a, Jinjun Wen ^a, Yu Zeng ^a, Mengyuan Li ^b, Yukun Tian ^a, Fan Yang ^{b,d},
Molly Meng-Jung Li ^c, Peirong Chen ^{a,e}, Haomin Huang ^{a,e}, Daiqi Ye ^{a,e}, Limin Chen ^{a,e,*}

^a Guangdong Provincial Key Laboratory of Atmospheric Environment and Pollution Control, School of Environment and Energy, South China University of Technology, Guangzhou 510006, China

^b State Key Laboratory of Catalysis, Dalian Institute of Chemical Physics, Chinese Academy of Sciences, Dalian 116023, China

^c Department of Applied Physics, The Hong Kong Polytechnic University, Hong Kong, China

^d School of Physical Science and Technology, ShanghaiTech University, Shanghai 201210, China

^e National Engineering Laboratory for VOCs Pollution Control Technology and Equipment, South China University of Technology, Guangzhou 510006, China

ARTICLE INFO

Keywords:

CO₂ hydrogenation to methanol
Cu-ZnO catalyst
Pressure effect
Strong metal-support interactions

ABSTRACT

Cu/ZnO-based catalysts have been extensively and intensively studied for CO₂ hydrogenation to methanol due to their relatively superior catalytic performance. However, the mediocre methanol selectivity over Cu/ZnO-based catalysts has not been disclosed mainly because the predominant by-product CO formation activity fails to arouse any attention, significantly deterring the further catalyst optimization. The ZnO_x-Cu nanoparticles (NP)-ZnO interface, derived from strong metal-support interactions (SMSI), has been recognized to be more active for methanol formation compared with the classical direct contact Cu-ZnO interface. In order to disclose the origin of the mediocre methanol selectivity, these two types of Cu-ZnO interfaces have been designed and constructed through carefully manipulating the synthesis and heat pre-treatment conditions of the powder model catalysts. Then, methanol and CO formation behaviors over these two interfaces have been explored thoroughly in actual reaction conditions. Finally, the origin of the mediocre methanol selectivity over Cu/ZnO-based catalysts has been proposed. This work provides unique insights for designing efficient Cu/ZnO-based catalysts with high methanol selectivity and yield and puts forward an effective strategy to investigate the catalytic behaviors over different interfaces in actual reaction conditions.

1. Introduction

Cu/ZnO-based catalysts are the most effective catalysts for CO₂ hydrogenation to methanol and have been investigated extensively and intensively [1–17]. Although researchers agree that there are synergistic effects between ZnO and Cu in Cu/ZnO-based catalysts, the roles of ZnO and the catalyst active site structures are still controversial [2,6,8–11, 14,18,19]. It is essential to reveal the active sites to suppress the generation of CO by-products through reverse water gas shift (RWGS) reaction to ensure high methanol selectivity and yield [20].

After decades of intensive investigation, several possible active sites related to the synergistic effects of Cu-ZnO catalysts have been proposed, where Zn exists in a metallic or oxidized state [2,21–24]. The earlier investigation reported that the surface Cu-Zn bimetallic alloys are the active sites for methanol synthesis [22–24]; however, Gotti and Prins

[21] proposed that CO₂ and water could prevent the formation of Cu-Zn alloys, and a recent study also demonstrated that Cu-Zn alloys preferred CO-rich reaction condition [11]. Further exploration found that metallic Zn will be partially oxidized to ZnO_x by ¹⁸O due to the dissociation of ¹⁸CO₂ in the CO₂-rich reaction condition, and the resulted ZnO_x-Cu phase promoted CO₂ hydrogenation through the preferred formate route [2, 19]. Similar oxidative Zn^{δ+} species was observed on the stepped Cu surface, leading to high methanol synthesis activity [25]. Therefore, the Zn species related to the active sites for methanol synthesis from CO₂ hydrogenation are regarded as partially oxidized state.

Currently, the active sites formed by partially oxidized Zn (namely, ZnO_x) covered on Cu NP are considered critical to methanol formation. Typically, the formation of ZnO_x overlayer is due to the strong metal-support interactions (SMSI), which proceeded through Zn species migration from bulk ZnO support to Cu NPs. The ZnO_x mainly exists as

* Correspondence to: School of Environment and Energy, South China University of Technology, Guangzhou 510006, China.

E-mail address: liminchen@scut.edu.cn (L. Chen).



disordered graphitic ZnOx overlayer covered on the Cu NPs [25,26]; subsequently, the metastable graphitic ZnOx species has been found to transform into dense and stable wurtzite ZnO nanocrystals during the reaction, accompanied with methanol synthesis activity decrease [27]. Furthermore, several studies have proposed that the SMSI-induced ZnOx-Cu NP-ZnO interface is more active in methanol production than the common non-covered Cu-ZnO interface [10,19,28–32]. Unfortunately, despite all the efforts in surface science and DFT simulation, material gap and pressure gap can't be excluded which is far away from the actual reaction conditions. In addition, it is very difficult to distinguish the two interfaces, i.e., Cu-ZnO interface (without ZnOx overlayer) and SMSI-induced ZnOx-Cu NP-ZnO interface, and their catalytic performance contribution in the supported Cu/ZnO-based powder catalysts system. Therefore, the rational design of powder model catalysts, including constructing and verifying these two interfaces, is essential but challenging.

Besides, methanol synthesis from CO₂ hydrogenation is normally operated at thermodynamically favorable high reaction pressure [4]. It is generally accepted that high pressure can shift the thermodynamic equilibrium and reaction kinetics towards methanol. Within the limited investigated pressure range in the laboratory, the methanol yield at thermodynamic equilibrium is found to increase with the reaction pressure [33]. Furthermore, a summary of previously reported catalytic performance of Cu/ZnO-based catalysts at different pressures indicates that methanol selectivity increases along with the reaction pressure (Fig. S1a). However, the effect of high pressure on the formation behavior of CO has not yet been clarified, and few publications have attempted to reveal the origin of the mediocre methanol selectivity of Cu/ZnO-based catalysts.

As reported, high pressure may alter the morphology and structure of Cu and ZnO species of the commercial Cu/ZnO/Al₂O₃ catalysts under CO₂ hydrogenation reaction conditions, for example, the aggregation and oxidation of Cu species [34–36], the agglomeration and partial reduction of ZnO species [37] as well as the oxidation of CuZn alloys [1, 2,4,38]. Such structural variations usually deactivate catalysts and decrease the methanol formation rate [2,4,35,37]. However, the structure evolutions with pressure increase remain rarely investigated, let alone the correlation with catalytic performance. Building the relationship between the structure evolutions and performance under varying reaction pressures will help understand the generally mediocre methanol selectivity of Cu/ZnO-based catalysts and accordingly develop highly efficient Cu/ZnO-based catalysts with superior methanol selectivity and yield.

Here, two Cu-ZnO catalysts with 1 wt% Cu, synthesized according to our recent publications [39,40], were calcined in different atmospheres to construct the Cu-ZnO model catalysts, which were subsequently

reduced in H₂ to generate different Cu-ZnO interfaces, i.e., the direct contact Cu-ZnO and the ZnOx-Cu NP-ZnO interfaces (see Scheme 1). The formation of these interfaces has been confirmed through SEM, XRD, Raman, EPR, quasi-in-situ XPS and in-situ FTIR characterizations. The catalyst performance and the corresponding micro-structure evolution have been further explored under different reaction pressures. According to the results, the correlation between the catalytic performance and structural characterizations at different reaction pressures has been revealed, which provides valuable guidelines for designing efficient Cu/ZnO-based catalysts with high methanol selectivity and yield.

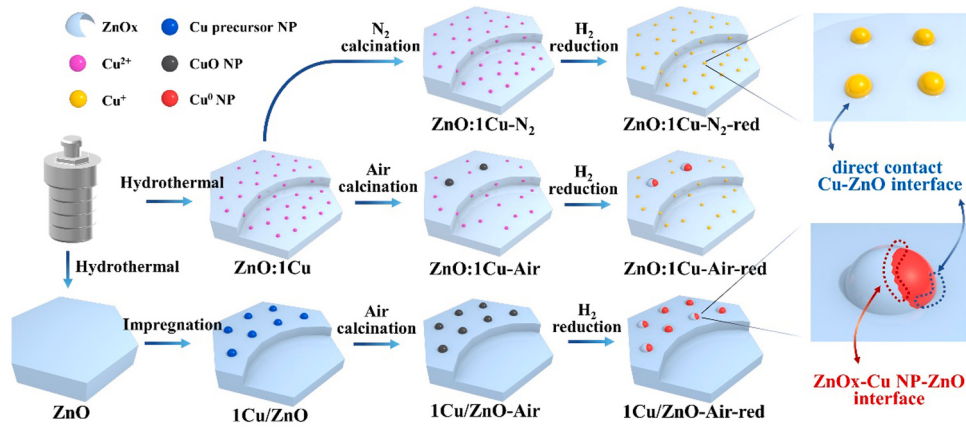
2. Experimental

2.1. Catalyst preparation

Pristine ZnO plates were prepared through hydrothermal method [41]. 6.3 g zinc acetate dehydrate (Zn(CO₂CH₃)₂, AR grade, Shanghai Aladdin) was completely dissolved in 60 mL deionized water, followed by addition of 1.6 g hexamethylenetetramine ((CH₂)₆N₄, AR grade, Guangzhou Chemical). The solution was stirred for 1 h and subsequently transferred into a 100-mL Teflon lined autoclave and maintained at 100 °C for 12 h. After the autoclave was cooled down to room temperature, the precipitate was collected, washed with deionized water and ethanol for several times and then dried at 80 °C for 12 h.

1 wt% Cu/plate ZnO model catalysts were prepared through impregnation. The calculated amount of copper acetate (Cu(CO₂CH₃)₂·H₂O, AR grade, Shanghai Aladdin) was completely dissolved in a small amount of deionized water, followed by addition of 2 g pristine ZnO plate and continuous stirring until the water evaporated completely. The sample was dried at 80 °C for 12 h, fully ground and calcined in dry air at 350 °C for 3 h, and the obtained model catalyst with Cu content of 1 wt% was denoted as 1Cu/ZnO-Air.

1 wt% Cu doped plate ZnO model catalysts were prepared through similar hydrothermal method with addition of copper nitrate trihydrate (Cu(NO₃)₂·3H₂O, AR grade, Shanghai Aladdin) in the solution. The uncalcined catalysts were fully ground and calcined in pure nitrogen or dry air at 350 °C for 3 h, and the obtained samples were denoted as ZnO:1Cu-N₂ and ZnO:1Cu-Air, respectively. Noted that the proper calcination conditions were determined by the thermogravimetric analysis (TGA) result presented in Fig. S2. Furthermore, TGA has also excluded the influence of residual surface metal salts on the catalytic performance and demonstrated the stable structure of ZnO:1Cu at high temperature.



* The lower and higher surface indicates the bulk and the surface of ZnO, respectively

Scheme 1. The construction procedures of different Cu-ZnO interfaces.

2.2. Catalyst characterization

Scanning electron microscopy (SEM) images and energy dispersive X-ray spectroscopy (EDS) for catalyst morphology and element distribution observation were obtained on a field emission scanning electron microscope (Carl Zeiss Merlin, Germany).

Thermogravimetric analysis (TGA) was carried out on a synchronous thermal analyzer (NETZSCH STA 449C, Germany) in dry air from 30 °C to 800 °C with a heating rate of 10 °C min⁻¹.

Electron paramagnetic resonance (EPR) spectra were obtained on an electron paramagnetic resonance spectrometer (Bruker A300, Germany) operated at 100 K, with a microwave power, modulation frequency, microwave frequency and modulation amplitude at 2.18 mW, 100 kHz, 9.33 GHz and 1.00 G, respectively.

X-ray diffraction (XRD) patterns were obtained on an X-ray diffractometer (Bruker D8 Advance, Germany) equipped with Cu K α radiation ($\lambda = 0.15418$ nm, 40 kV, 40 mA) and recorded in the 2 θ range from 20° to 80°.

Visible Raman spectra were obtained on a Raman spectrometer (HORIBA LabRAM HR Evolution, France), equipped with a CCD detector and a HeNe laser (532 nm), and recorded in the range of 200–800 cm⁻¹.

Quasi-in-situ X-ray photoelectron spectroscopy (XPS) was obtained on an electronic spectrometer (Thermo Fisher Scientific EscaLab Xi⁺, US) with Al K α (1486.6 eV) as the excitation source. The Cu 2p, Zn 2p, O 1s and C 1s XPS spectra were recorded for all samples and the corresponding binding energies (BE) were corrected by C 1s at 284.8 eV. The samples were calcined in the treatment chamber in dry air at 350 °C for 3 h, followed by transfer to the analysis chamber for detection; then the calcined samples were transferred back to the treatment chamber for reduction in 5% H₂/Ar at 300 °C for 3 h, followed by transfer to the analysis chamber for second detection. All operations were carried out under vacuum conditions to prevent samples from being oxidized.

H₂ temperature-programmed reduction (H₂-TPR) was performed on an automated chemisorption analyzer (Micromeritics AutoChem II 2920, US). 100 mg calcined catalyst was placed in a U-shaped quartz tube and flushed in pure Ar at 300 °C for 1 h with a flow rate of 30 mL·min⁻¹ and heating rate of 5 °C·min⁻¹, followed by cooling to 45 °C. The sample was subsequently flushed with 5% H₂/Ar until the baseline was stable. Afterwards, the data were recorded by TCD with a heating rate of 5 °C min⁻¹ from 45 °C to 800 °C.

In-situ Fourier transform infrared (in-situ FTIR) spectra were obtained on a Fourier transform infrared spectrometer (Thermo Electron Nicolet 6700, US) equipped with an MCT detector. The sample was pretreated with 0.1 mbar O₂ stream at 300 °C for 30 min, followed by vacuum annealing at 300 °C for 30 min. After cooling to room temperature, the background spectrum was recorded, and then the H₂ reduction treatment was carried out (1 mbar, 100, 200, 300 °C, 30 min for each temperature). CO adsorption was carried out at room temperature with 0.001 mbar and 0.01 mbar CO streams for 10 min, respectively. The spectra (32 scans) with a resolution of 4 cm⁻¹ were continuously recorded.

CO₂ temperature-programmed desorption (CO₂-TPD) was performed on an automated chemisorption analyzer (Micromeritics AutoChem II 2920, US), connected with an on-line mass spectrometer (Hiden Analytical HPR 20, UK). 200 mg calcined catalyst was placed in a U-shaped quartz tube and reduced at 300 °C for 3 h in 5% H₂/Ar with a flow rate of 30 mL·min⁻¹ and heating rate of 5 °C·min⁻¹, followed by cooling to 45 °C in pure Ar. The sample was subsequently saturated with 20% CO₂/Ar for 1 h and flushed with pure He until the baseline was stable. Afterwards, the experiment was performed in He stream from 45 °C to 800 °C with a heating rate of 5 °C·min⁻¹, while the desorbed CO₂ was detected by the on-line MS detector.

2.3. Catalyst performance evaluation

Catalytic activity evaluation of CO₂ hydrogenation to methanol was

performed on a self-made high-pressure, continuous-flow, fixed-bed reactor combined with a gas chromatograph (Shimadzu GC-2014C, China). 500 mg catalyst was placed in a stainless-steel tube and pre-reduced in 5% H₂/Ar at 300 °C for 3 h, followed by cooling to room temperature. The reaction conditions were controlled as following: 200–300 °C, V(H₂):V(CO₂):V(N₂) = 69:23:8 and GHSV = 3600 mL·g⁻¹·h⁻¹. The reactants and products were detected by the on-line gas chromatograph, which was equipped with FID and TCD detection channels. The CO₂ conversion, methanol selectivity and product yields were calculated according to our previous publications [39].

3. Results and discussion

3.1. Construction of different Cu-ZnO interfaces and their characterizations

The synthesis processes of Cu-ZnO model catalysts were illustrated in Scheme 1. The pristine ZnO plates were prepared through hydrothermal method. The 1 wt% Cu/ZnO (1Cu/ZnO) model catalyst was prepared through impregnation, then calcined in dry air and denoted as 1Cu/ZnO-Air. The other ZnO:1 wt% Cu (ZnO:1Cu) model catalyst was prepared through hydrothermal method similar to that of pristine ZnO plates in the presence of Cu precursor, then calcined in pure nitrogen and denoted as ZnO:1Cu-N₂. Besides, ZnO:1Cu-Air, the control sample, was obtained by calcination of ZnO:1Cu in dry air. All Cu-ZnO catalysts contain 1 wt% Cu, verified by ICP characterization. More detailed synthesis information is shown in the catalyst preparation section. The SEM images of the pristine ZnO plate and Cu-ZnO model catalysts (1Cu/ZnO and ZnO:1Cu) are presented in Fig. S3. The pristine ZnO exhibits a typical hexagonal plate-like structure with particle size and thickness in the range of 3.0–5.5 μ m and 1.0–1.5 μ m, respectively. The hexagonal shape of the ZnO plate as well as its size can be preserved after impregnation with Cu (Fig. S3b). Interestingly, the size and thickness decreased significantly after introducing Cu via the hydrothermal method (Fig. S3c), though the hexagonal plate-like structure can be remained. The decrease of the ZnO size in ZnO:1Cu may be due to the distortion originated from substitution of Cu dopant in the host ZnO lattice [42].

Fig. 1a displays the EPR spectra of the pristine ZnO plate and ZnO:1Cu catalyst. The resonance at $g = 1.953$, attributed to the shallow donor centers caused by the interstitial Zn (Zn_i) [43,44], was weakened in ZnO:1Cu, indicating the incorporation of Cu ions into the Zn_i sites [45]. Additionally, the hyperfine structure ($g_{\parallel} = 2.384$ and $g_{\perp} = 2.095$) observed in ZnO:1Cu means the doping of Cu²⁺ into the ZnO lattice [46–48]. ZnO:1Cu was then calcined at 350 °C (determined on the basis of TGA results, Fig. S2) in pure N₂ before undergoing H₂ reduction at 300 °C; SEM images of the corresponding calcined and reduced ZnO:1Cu model catalysts are shown in Figs. 1b and c. Neither CuO nor Cu particles could be observed on the catalyst surface, whereas the EDS element mapping of the reduced ZnO:1Cu-N₂ demonstrates homogeneous distribution of Cu (Fig. 1d), indicating the successful doping of Cu into the bulk of the ZnO plate in ZnO:1Cu-N₂. Besides, no diffraction at $2\theta = 43.3^\circ$ attributed to Cu (111) crystal phase over the reduced ZnO:1-Cu-N₂ can be observed in XRD patterns (Fig. S4), while XPS Cu LMM spectrum (Fig. S5b) and H₂-TPR experiment (Fig. S6 and Table S3) indicate the Cu²⁺ species in ZnO:1Cu-N₂ will be reduced to Cu⁺ rather than metallic copper. Therefore, the above analysis has confirmed the high dispersion of the doped Cu species in the bulk of ZnO:1Cu-N₂.

Fig. 2 shows SEM images of the calcined and reduced 1Cu/ZnO-Air model catalysts. CuO particles with the size of 12.5 nm are uniformly distributed on the surface of 1Cu/ZnO catalyst after calcination in air (Fig. 2a and b). After H₂ treatment, they are reduced to Cu NPs with the size of 15.2 nm (Fig. 2c and d). XRD patterns (Fig. S4) also display the diffraction at $2\theta = 43.3^\circ$ attributed to Cu (111) crystal phase in the reduced 1Cu/ZnO-Air catalyst. The SEM images (Fig. 2c and d), EDS element mapping (Fig. 2c) and XRD pattern (Fig. S4) together prove that

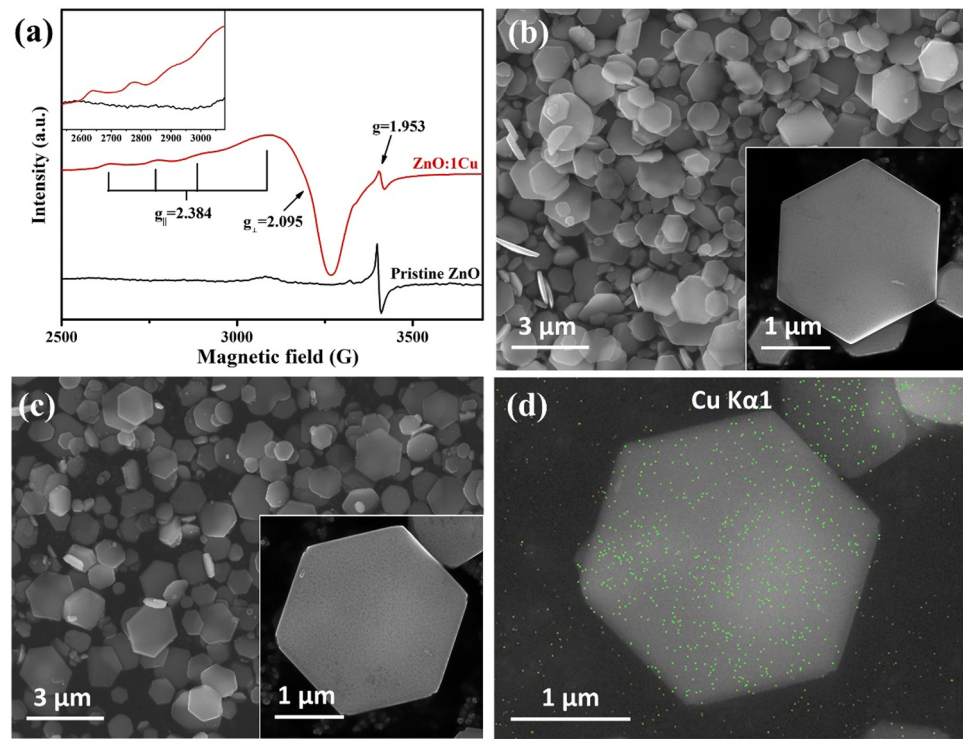


Fig. 1. (a) EPR spectra of the pristine ZnO plate and ZnO:1Cu catalyst. SEM images of (b) ZnO:1Cu-N₂ model catalyst and (c) the reduced ZnO:1Cu-N₂ model catalyst. (d) Corresponding EDS element mapping of (c).

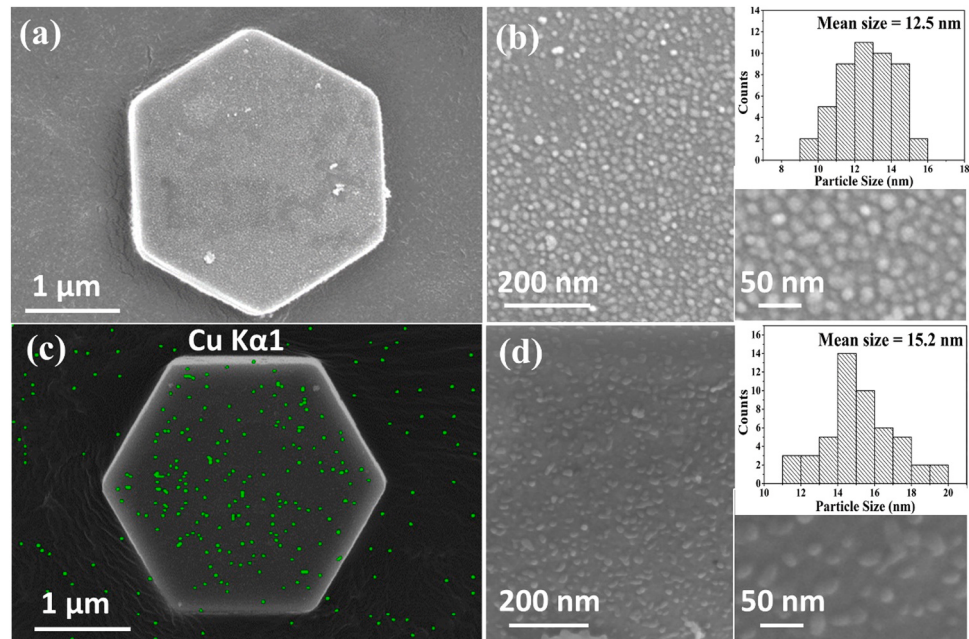


Fig. 2. (a) SEM images and (b) the local enlarged views with corresponding particle size distribution of copper species of 1Cu/ZnO-Air model catalyst. (c) EDS element mapping and (d) the local enlarged views with corresponding particle size distribution of copper species of the reduced 1Cu/ZnO-Air model catalyst.

Cu NPs are uniformly dispersed on the ZnO surface in the reduced 1Cu/ZnO-Air catalyst. Interestingly, in the case of ZnO:1Cu-Air catalysts calcined at 350 °C in dry air, CuO particles can also be found on the surface of the ZnO plate (Fig. S7a) due to the partial segregation of Cu from the bulk during calcination in air, which are then reduced to Cu NPs upon H₂ reduction (Fig. S7b). Accordingly, ZnO:1Cu-Air contains both doped Cu species in the bulk ZnO and Cu NP on the surface simultaneously, thus is regarded as a control sample.

To confirm the formation of ZnOx overlayer on the surface Cu NPs during the reduction, quasi-in-situ XPS was performed to explore the evolution of the amount and chemical state of surface elements in the Cu-ZnO model catalysts. Fig. S5 presents the XPS Cu 2p, Cu LMM, Zn 2p and Zn LMM spectra of the ZnO:1Cu-N₂ and the 1Cu/ZnO-Air catalysts after in-situ calcination and reduction. The binding energy (BE) shifts of Cu 2p (1.5 eV) and Zn 2p (0.6 eV) of 1Cu/ZnO-Air are larger than that of ZnO:1Cu-N₂ (0.3 eV and 0 eV, respectively) after reduction, indicating

the possible stronger metal-support interactions between surface Cu NPs and ZnO in 1Cu/ZnO-Air [49]. Accordingly, the amounts of surface Cu, Zn, and O, derived from XPS analysis, are shown in Table 1. For ZnO:1Cu-N₂, the atomic ratio of Cu is 8.56%, which is greater than the loading amount of 1 wt% obtained through ICP, indicating most doped Cu species is located near the surface. The atomic ratio of Zn/(Cu+Zn) in ZnO:1Cu-N₂ remains basically the same during the heat treatment processes, demonstrating no obvious segregation of Zn species in ZnO:1-Cu-N₂ during reduction. On the other hand, the atomic ratio of Zn/(Cu+Zn) in 1Cu/ZnO-Air increases significantly from 77.56% to 86.42%. This phenomenon demonstrates the migration of Zn species from the bulk of ZnO support to the surface of Cu NPs in 1Cu/ZnO-Air, leading to the enrichment of ZnOx species on the surface of Cu NPs.

In order to further verify the migration of ZnOx to the surface of Cu NP in reducing atmosphere, in-situ FTIR of CO adsorption was carried out. 1Cu/ZnO-Air turned totally black after reduction in H₂ and infrared signals can hardly be detected. Then, the control sample, ZnO:1Cu-Air after O₂ oxidation at 300 °C, was selected to conduct CO adsorption. The corresponding in-situ FTIR of CO adsorption spectra are presented in Fig. 3. The vibration peaks at 2111 and 2088 cm⁻¹ can be attributed to the adsorption of CO on Cu⁺ (CO-Cu⁺) and metal Cu⁰ (CO-Cu⁰), respectively [50,51]. After reduction at 100 °C, the CO-Cu⁺ adsorption peak is weakened, indicating that part of Cu⁺ is reduced to Cu⁰. As the reduction temperature increases, both the CO-Cu⁺ and CO-Cu⁰ adsorption peaks are significantly weakened and eventually completely disappear at 300 °C. This indicates the increasing migration of ZnOx and covers the surface of Cu NPs accordingly due to the SMSI between surface Cu NPs and ZnO, which is consistent with the result of the quasi-in-situ XPS characterization of 1Cu/ZnO-Air under the same conditions as in-situ FTIR experiment, as displayed in Fig. S8 and Table S4. Fig. 3b shows the in-situ FTIR spectra of ZnO:1Cu-Air after H₂ reduction at 300 °C followed by re-oxidation in O₂ at 300 °C. The reappearance of CO-Cu⁺ adsorption peak demonstrates that the ZnOx species covered on Cu NP will migrate back to the bulk ZnO during oxidation treatment to re-expose Cu NP. These have disclosed the well reversible migration behavior of the ZnOx species, and further confirmed the formation of ZnOx overlayer on the surface Cu NPs.

Fig. 3c presents the XPS O 1s spectra of the model catalysts after calcination and reduction. All O 1s spectra were deconvoluted to two peaks consisting of the lattice oxygen anion O²⁻ in the wurtzite structure (O_L) and the chemisorbed oxygen species at surface defects (O_S) with BE in the range of 529.9–530.2 eV and 531.5–531.9 eV, respectively [52]. The atomic ratio of O_S species in 1Cu/ZnO-Air is 17.00%, significantly higher than that in ZnO:1Cu-N₂ (13.05%), suggesting a higher concentration of surface oxygen vacancies in 1Cu/ZnO-Air. The same conclusion can also be elucidated from the highest E₁(LO)/E₂^{high} peak intensity ratio of 1Cu/ZnO-Air in Raman (Fig. S9). After reduction, the ratio of O_S species in ZnO:1Cu-N₂ remains basically the same, while it increases significantly from 17.00% to 20.73% in 1Cu/ZnO-Air. This should be due to the migration of ZnOx species to the surface, accompanied with the formation of oxygen vacancies [40]. In short, quasi-in-situ XPS and

in-situ FTIR has confirmed the formation of ZnOx overlayer on the surface Cu NPs during the reduction.

Above investigation confirms that Cu species are doped into the bulk of ZnO in ZnO:1Cu-N₂ without obvious Cu species on the surface; the interface with doped Cu in ZnO, without ZnOx overlayer, is regarded as the direct contact Cu-ZnO interface. Accordingly, Cu NPs are uniformly loaded on the surface of 1Cu/ZnO-Air; Cu NPs will be encapsulated by the ZnOx species during reduction and form the interface defined as ZnOx-Cu NPs-ZnO interface. Besides, there should be some mixing layers between Cu and ZnO species in the contact area of Cu NPs and ZnO support, which is similar to that of Cu doped ZnO and considered as the direct contact Cu-ZnO interface as well. For the control sample ZnO:1Cu-Air, while containing the direct contact Cu-ZnO interface, calcination in air results in partial segregation of Cu from the bulk ZnO (Figs. S6 and S7), thereby also forming some ZnOx-Cu NP-ZnO interface during reduction. Thus, two interfaces, i.e., the direct contact Cu-ZnO interface and the ZnOx-Cu NP-ZnO interface, are successfully constructed as illustrated in Scheme 1.

3.2. Catalytic performance over different Cu-ZnO model catalysts and interfaces

Fig. 4 displays the catalytic performance of CO₂ hydrogenation to methanol at 3 MPa over Cu-ZnO model catalysts. At the same temperature, both CO₂ conversion and methanol yield over 1Cu/ZnO-Air are higher than those of ZnO:1Cu model catalysts (Fig. 4a and b); furthermore, 1Cu/ZnO-Air has the highest methanol selectivity at the same CO₂ conversion, while ZnO:1Cu-N₂ has the poorest one (Fig. 4c). It is worth mentioning that 1Cu/ZnO-Air also shows higher CO₂ conversion in RWGS reaction than ZnO:1Cu-N₂ at atmospheric pressure (Fig. S10a). The better activity over 1Cu/ZnO-Air should be related to the larger amount of activated CO₂ adsorption species (Fig. S11) associated with the abundant oxygen vacancies, originated from the stronger metal-support interactions between Cu NPs and ZnO support as proved by Raman (Fig. S9) and XPS (Fig. 3c) analysis. In order to further explore the performance over the investigated two interfaces, the CO and methanol formation rates (R_{SSA}, $\mu\text{mol}_{\text{product}}\text{s}^{-1}\text{m}^{-2}$) at 3 MPa were calculated through special algorithms (SI, calculation section), and the results are illustrated in Fig. 4d. Intuitively, the total activity of CO₂ hydrogenation (CH_3OH R_{SSA} + CO R_{SSA}) over the ZnOx-Cu NP-ZnO interface is much higher than that of the direct contact Cu-ZnO interface, and increases faster along with the temperature increase. However, the methanol formation rate (CH_3OH R_{SSA}) over the ZnOx-Cu NP-ZnO interface is only slightly higher than that over the direct contact Cu-ZnO interface. On the contrary, CO formation rate (CO R_{SSA}) is significantly higher than that over the direct contact Cu-ZnO interface, especially at temperatures above 260 °C. This means methanol selectivity over the ZnOx-Cu NP-ZnO interface should be inferior to that over the direct contact Cu-ZnO interface at high temperature. The lower methanol selectivity over the ZnOx-Cu NP-ZnO interface may originate from its higher catalytic activity caused by thermodynamic equilibrium. Considering that high pressure facilitates methanol formation from the thermodynamics perspective [33], in order to find out the potentiality of the ZnOx-Cu NP-ZnO interface on methanol selectivity to enhance methanol yield over supported Cu/ZnO catalysts, it is critical to investigate methanol formation at suitable temperature (with high methanol yield below thermodynamic equilibrium temperature) and high temperature (above thermodynamic equilibrium temperature) under various high pressures.

The previously reported catalytic performance of Cu/ZnO-based catalysts at different pressures was summarized in Fig. S1. As presented, both methanol selectivity and yield increase with reaction pressure; at the same pressure, higher CO₂ conversion is generally accompanied with higher methanol yield but lower methanol selectivity. In contrast, no obvious correlation between pressure variation and CO yield can be observed. Then, methanol and CO formation rates

Table 1
Surface composition based on quasi-in-situ XPS experiments (Figs. 3c and S5).

Samples	Surface composition (%) ^a			O atomic ratio (%) ^b	
	Cu/ (Cu+Zn)	Zn/ (Cu+Zn)	Variance ^c	O _L	O _S
ZnO:1Cu-N ₂	Cal	8.56	91.44	-0.05	86.95 13.05
	Red	8.34	91.66		87.69 12.31
1Cu/ZnO-Air	Cal	22.44	77.56	8.86	83.00 17.00
	Red	13.58	86.42		79.27 20.73

^a Calculated from Zn 2p and Cu 2p.

^b Calculated from O 1s.

^c Zn/(Cu+Zn) value of the reduced sample subtracted the corresponding calcined sample.

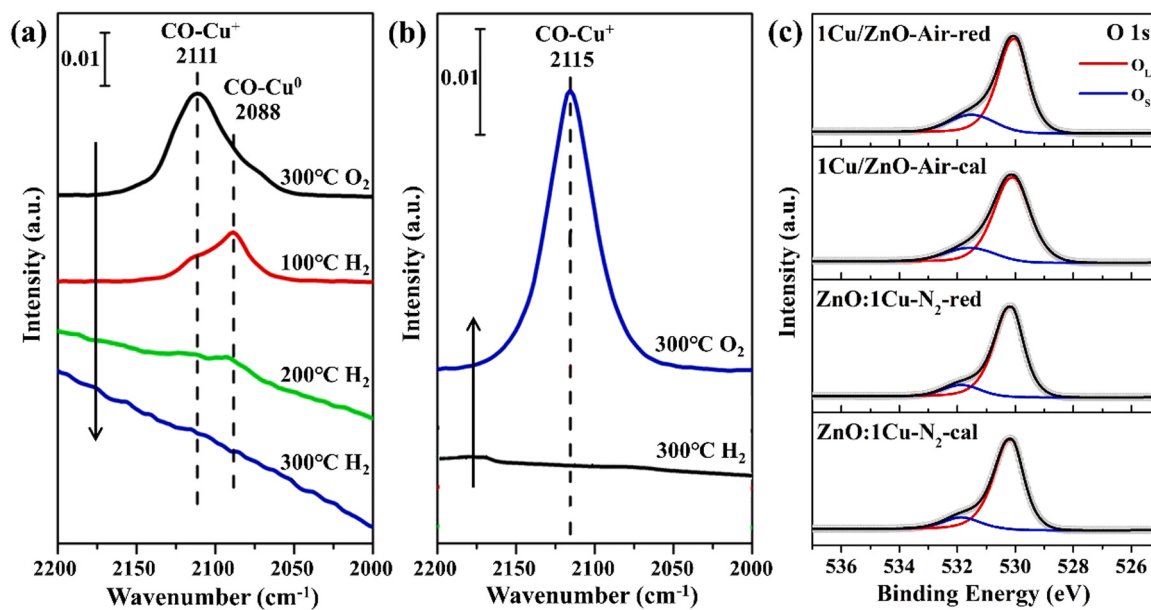


Fig. 3. In-situ FTIR spectra of CO adsorption at RT on ZnO:1Cu model catalyst (a) after O₂ treatment and vacuum annealing at 300 °C followed by H₂ reduction at a different temperature; (b) after H₂ reduction at 300 °C followed by O₂ treatment and vacuum annealing at 300 °C. (c) Quasi-in-situ XPS O 1s spectra of the Cu-ZnO model catalysts after in-situ calcination and reduction.

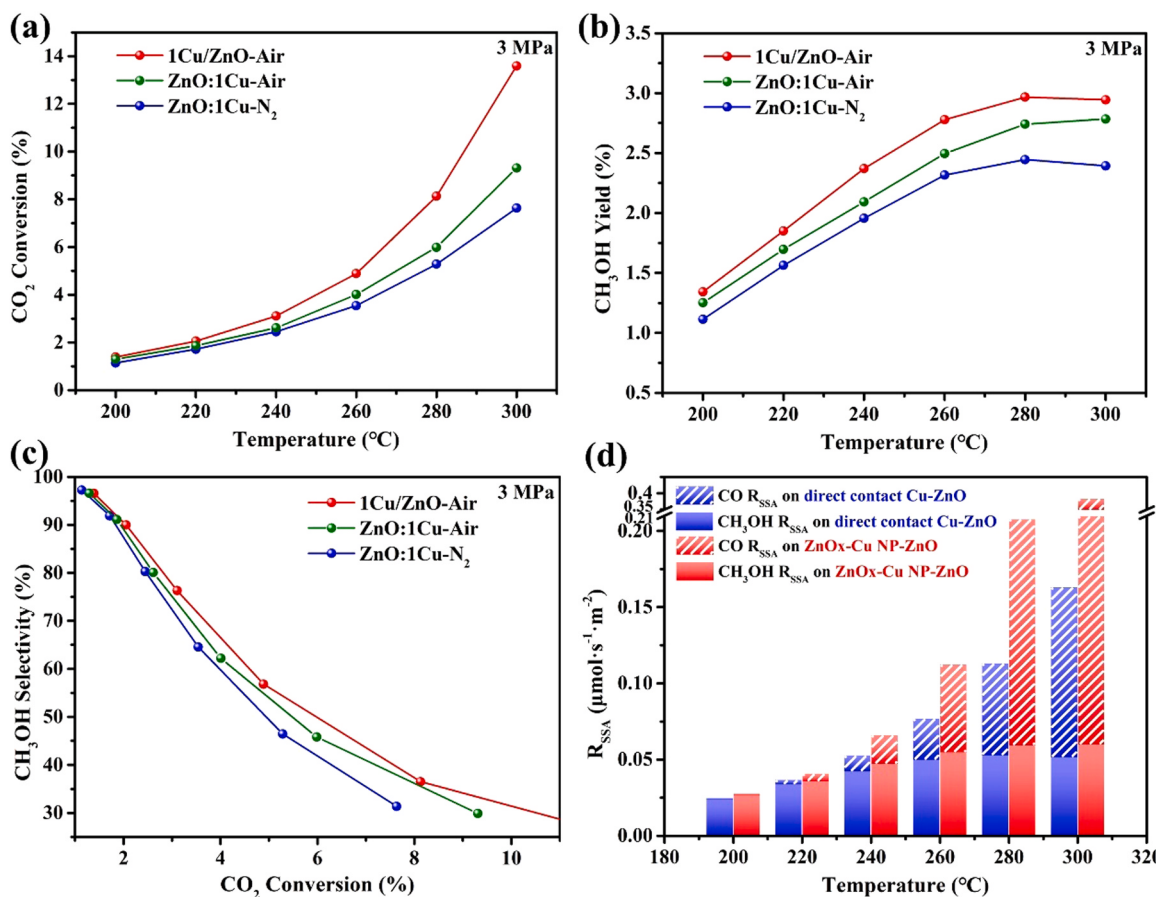


Fig. 4. Catalytic performance for CO₂ hydrogenation to methanol over Cu-ZnO model catalysts: (a) CO₂ conversion, (b) methanol yield, (c) methanol selectivity corresponding to the CO₂ conversion and (d) product formation rates (Reaction conditions: P = 3.0 MPa, H₂/CO₂/N₂ = 69/23/8 (v/v/v), WHSV = 3600 mL•g_{cat}⁻¹•h⁻¹).

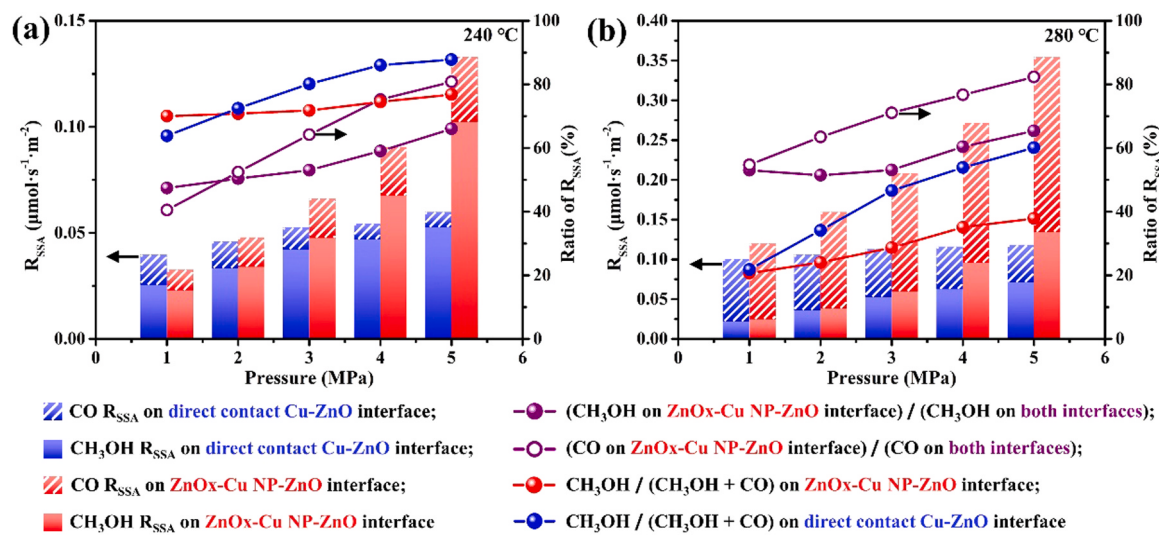


Fig. 5. R_{SSA} of CO and CH_3OH over different interfaces and their ratios at (a) 240 and (b) 280 °C (Reaction conditions: $H_2/CO_2/N_2 = 69/23/8$ (v/v/v), WHSV = 3600 $mL \cdot g_{cat}^{-1} \cdot h^{-1}$).

over the two investigated interfaces at different pressures at 240 °C (suitable temperature with mild RWGS reaction) and 280 °C (high temperature with severe RWGS reaction) were further investigated and illustrated (Figs. S12, S13 and 5). At 240 °C and low reaction pressures (1–2 MPa), methanol formation rates over the ZnOx-Cu NP-ZnO interface and the direct contact Cu-ZnO interface are comparable; as the pressure continues rising to 5 MPa, it increases promptly and obviously faster over the former, leading to significant increase in its contribution to the total methanol formation rate from 50.4% at 2 MPa to 66.0% at 5 MPa at 240 °C (purple line with solid circle). This demonstrates the ZnOx-Cu NP-ZnO interface plays paramount roles in methanol formation at high pressure compared with the direct contact Cu-ZnO interface. CO formation rate over the ZnOx-Cu NP-ZnO interface also increases along with pressure, but interestingly, it decreases gradually over the direct contact Cu-ZnO interface. As a result, the contribution of the ZnOx-Cu NP-ZnO interface to the total CO formation rate is up to 80.8% at 5 MPa at 240 °C (purple line with hollow circle). The joint increase of methanol and CO formation rates over the ZnOx-Cu NP-ZnO interface results in slight methanol selectivity increase from 70.0% at 1 MPa to 76.8% at 5 MPa at 240 °C (red line with solid circle) and from 20.7% at 1 MPa to 37.9% at 5 MPa at 280 °C. In contrast, methanol selectivity over the direct contact Cu-ZnO interface is higher and increases faster (blue line with solid circle). Compared with the direct contact Cu-ZnO interface, the inferior methanol selectivity at high pressure over the ZnOx-Cu NP-ZnO interface, the paramount contributor, indicate that the methanol formation rate increase along with pressure is suppressed by the faster CO formation rate at high pressure, irrespective its higher activity for both methanol and CO formation. In order to disclose the origin of different methanol and CO formation behaviors over the two investigated interfaces, more characterization combined with catalytic performance tests has been explored.

3.3. Discussion

Above catalytic performances indicate thermodynamic limitation or CO further hydrogenated to methanol is less paramount over the ZnOx-Cu NP-ZnO interface, finally resulting in unsatisfactory mediocre methanol selectivity over supported Cu/ZnO-based catalysts. To disclose the influences of the formed CO on methanol formation over different interfaces, the catalytic performance of Cu-ZnO model catalysts for CO hydrogenation to methanol at 3 MPa was evaluated (Fig. S14), and the influence of the CO concentration in the feed gas has been explored according to the reported literature as well [5,53,54]. Extremely

deficient CO hydrogenation activity is found over ZnO:1Cu-N₂, indicating that methanol prefers to be produced through direct hydrogenation of CO_2 over the direct contact Cu-ZnO interface; when pressure increases, RWGS reaction should be suppressed, leading to the significant methanol selectivity increase. On the other hand, the low CO hydrogenation activity over 1Cu/ZnO-Air indicates severe RWGS reaction over the ZnOx-Cu NP-ZnO interface and that formate route is the probable main methanol synthesis route; when pressure increases, RWGS reaction and formate route should be promoted together, leading to the slight methanol selectivity increase. The CO concentration in the feed gas varies within 1% (Fig. S15), and the resulted relative variation ratio of methanol yield should be no more than 5% [5,16], excluding the influence of CO concentration on methanol yield. As mentioned in the Introduction section, different micro-structures may have been induced at the interfaces at high reaction pressure.

3.3.1. The catalyst micro-structure evolution along with reaction pressures

Recently, both activation atmosphere and reaction conditions have been reported to influence the micro-structures of Cu-ZnO catalysts [1,3, 34–38]. It has been recognized that CuZn alloys will not be formed during reduction at atmospheric pressure and will be continuously oxidized during high-pressure CO_2 hydrogenation reactions (evidenced by in-situ and operando X-ray absorption spectroscopy) [1,2,4,38]. Figs. 6 and S16 present the XPS Zn 2p and Zn LMM spectra of all the Cu-ZnO model catalysts after reaction at different pressures, respectively. Both shape and position of the Zn 2p peaks of all used 1Cu/ZnO-Air catalysts are essentially the same (Fig. 6a). The steady atomic ratios of Zn/(Cu+Zn) at different reaction pressures (Table S6) indicate the ZnOx-Cu NP-ZnO interface maintains its structure well when the pressure increases.

As far as ZnO:1Cu-N₂ (Fig. 6b), at the beginning, the Zn 2p_{3/2} spectra consist a single peak at 1021.5 eV, which is ascribed to Zn^{2+} in the wurtzite ZnO phase [55]. However, when the reaction pressure increases further, the single peak splits into two peaks towards lower and higher BEs located at around 1020.8 and 1022.9 eV, respectively, with the intensity of the former decrease and that of the latter increase gradually. According to the limited difference in Zn LMM spectra (Fig. S16), the existence of Zn^0 species can be excluded. Then, the peak at BE of 1020.8 eV should be ascribed to the Zn^{2+} species with BE red-shifted due to the reduced charge transfer from Zn to O in high-pressure H_2 [56–60]. The additional peak with BE at 1022.9 eV should be ascribed to the hydroxylated Zn^{2+} species (ZnOH) [61,62]. Its intensity increase is concomitant with the decrease in that of wurtzite

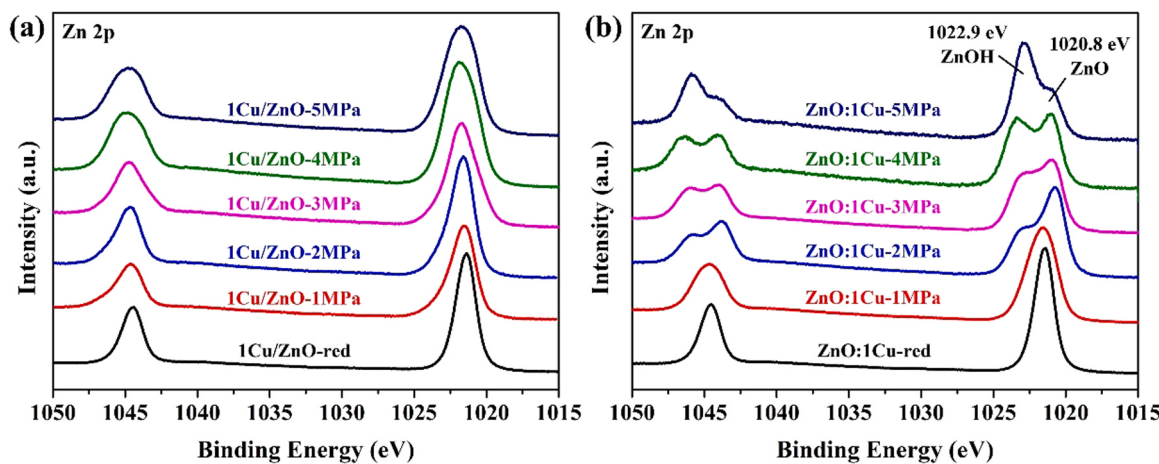


Fig. 6. XPS Zn 2p spectra of the Cu-ZnO model catalysts after high-pressure reaction: (a) 1Cu/ZnO-Air and (b) ZnO:1Cu-N₂.

Zn²⁺, indicating the transformation of ZnO to ZnOH at elevated reaction pressures. It has been reported that H₂ undergoes heterolytic dissociation at surface O and Zn sites to generate O-H and Zn-H species, in which the chemisorbed H species at O sites is more stable, while H species at the Zn-H sites will further migrate to nearby O sites and form another O-H species due to the low energy barriers [63]. This kind of H₂ dissociation is pressure dependent [9,64], thus more ZnOH species can be detected as the reaction pressure increases (Fig. 6b). In addition, the Cu⁺ species in the reduced ZnO:1Cu-N₂ catalyst presents a high energy barrier and contributes very little to H₂ dissociation [15,65]. Consequently, ZnO:1Cu-N₂ is more likely to work like oxide catalysts in methanol synthesis from CO₂ hydrogenation rather than Cu-based catalysts, in which the adsorbed CO₂ prefers to seize H species at the Zn-H sites instead of O-H sites to form HCOO* and H₂COO* species due to the extremely low energy barriers [66–68]. Therefore, ZnOH species is possible to be accumulated on the surface of ZnO:1Cu-N₂, indicating the lower CO₂ hydrogenation activity.

It should be noted that unlike ZnO:1Cu-N₂, no signal of ZnOH in 1Cu/ZnO-Air after high-pressure reaction has been detected (Fig. 6a). This is because the surface Cu⁰ NPs can promote H₂ dissociation and

spillover easily, induce more reactions and significantly reduce the energy barriers of H₂COOH* cleavage and subsequent dehydration, seizing more H species at the O-H sites and consuming ZnOH [69,70].

3.3.2. Methanol and CO formation behaviors at high pressure over the investigated interfaces

On the basis of the above investigation, both methanol and CO formation behaviors in CO₂ hydrogenation over the ZnOx-Cu NP-ZnO interface and the direct contact Cu-ZnO interface are put forward and illustrated in Fig. 7. For the ZnOx-Cu NP-ZnO interface induced by SMSI, H₂ dissociative adsorption is greatly enhanced because of the existence of Cu⁰ NPs, which promote spillover and provides active H* species required for CO₂ hydrogenation [69], thus assisting the hydrogenation of intermediate species through both formate route and RWGS reaction. When reaction pressure increases, both methanol and CO formation rates over the ZnOx-Cu NP-ZnO interface are significantly improved, leading to relatively inferior methanol selectivity (Fig. 5). For the direct contact Cu-ZnO interface, the accumulation of ZnOH at elevated reaction pressures indicates that its CO₂ hydrogenation reaction mechanism is similar to that of oxide catalysts, in which H₂ undergoes heterolytic

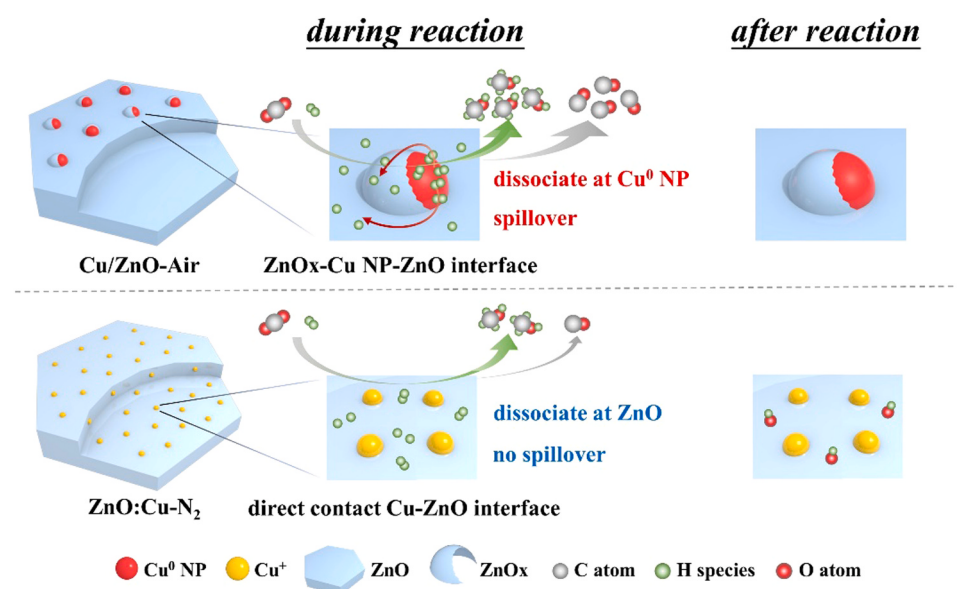


Fig. 7. Illustrative diagram of CO₂ hydrogenation reaction over different Cu-ZnO interfaces.

dissociation at ZnO rather than Cu⁺ species. Due to the lack of active atomic H* provided through spillover from Cu⁰ NPs, CO₂ hydrogenation over the direct contact Cu-ZnO interface is not as active as that over the ZnOx-Cu NP-ZnO interface; besides, the accumulated ZnOH may occupy some of the active sites. Furthermore, the high energy barrier of CO₂ hydrogenation to carboxylate over oxides catalysts may lead to lower CO formation rate [68]. Accordingly, the direct contact Cu-ZnO interface exhibits significantly poorer CO₂ conversion, methanol formation rate and relatively higher methanol selectivity at elevated reaction pressures (Fig. 5).

3.3.3. The origin of mediocre methanol selectivity of Cu/ZnO-based catalysts for CO₂ hydrogenation

The supported powder Cu/ZnO-based catalysts, represented by the designed supported model catalyst 1Cu/ZnO-Air, consist of both the direct contact Cu-ZnO interface and the ZnOx-Cu NP-ZnO interface. At 240 °C, before reaching the thermodynamic equilibrium, they exhibit comparable methanol formation rates as well as CO formation rates at pressures below 3 MPa; then both methanol and CO formation rates increase much more promptly over the ZnOx-Cu NP-ZnO interface at higher reaction pressures above 3 MPa. The accelerated methanol formation rate is accompanied with the faster CO formation rate owing to low CO hydrogenation activity, and thus the methanol selectivity over the ZnOx-Cu NP-ZnO interface remains mediocre with pressure increase. Accordingly, at 5 MPa, the ZnOx-Cu NP-ZnO interface displays higher contribution to both methanol (66.0%) and CO formation (80.8%) compared with the direct contact Cu-ZnO interface, and they increase by 24.5% and 25.9%, respectively compared with that at 3 MPa. In addition, industrial methanol synthesis is normally operated at 10–15 MPa, much higher than the investigated reaction pressure. The ZnOx-Cu NP-ZnO interface should exhibit far superior formation rates for both methanol and CO, thus acting as the paramount contributor to methanol formation but only inferior methanol selectivity can be obtained. As a result, the mediocre methanol selectivity of Cu/ZnO-based catalysts should originate from the severe CO formation over the ZnOx-Cu NP-ZnO interface at elevated pressure.

The ZnOx-Cu NP-ZnO interface contributes much more to methanol yield but with lower selectivity while the direct contact Cu-ZnO interface with poor activity but higher methanol selectivity contributes less to methanol yield at high reaction pressures. In order to further improve methanol selectivity of Cu/ZnO-based catalysts, it is essential to explore the micro-structures of the ZnOx-Cu NP-ZnO interface to identify methanol and CO formation sites and the evolution of intermediate species under actual operation conditions. These require in-situ and operando surface characterization technologies with atomic level resolution at high working pressure. In addition, the constructed powder model catalysts should be suitable for these surface characterization technologies. Even the micro-structures of the active sites for methanol and CO formation can be disclosed at atomic level, it is still a challenge to fine regulate the preparation parameters to synthesize the expected micro-structures. This may be the reasons that although many efforts have been devoted to revealing the active site structure for further enhancing the catalytic performance, the highly active and selective Cu/ZnO-based catalysts for CO₂ hydrogenation are still lacking. Looking for other efficient non-Cu/ZnO-based catalysts should be a more reasonable option.

4. Conclusion

In order to disclose the origin of the mediocre methanol selectivity of Cu/ZnO-based catalysts for CO₂ hydrogenation to methanol under actual reaction conditions, the direct contact Cu-ZnO interface and the ZnOx-Cu NP-ZnO interface were constructed and well distinguished through carefully manipulating the synthesis and heat pre-treatment conditions of the ZnO:1Cu-N₂ and 1Cu/ZnO-Air powder model catalysts, and their catalytic performance for methanol and CO formation in

CO₂ hydrogenation at different reaction pressures has been explored. The ZnOx-Cu NP-ZnO interface displays both higher methanol and CO formation activity at elevated pressure than that of the direct contact Cu-ZnO interface, owing to the ZnOx overlayer originating from SMSI. As the reaction pressure increases from 1 to 5 MPa, the ZnOx-Cu NP-ZnO interface displays much higher methanol formation rate, thus playing paramount roles in methanol formation; however, it also results in severe CO formation, leading to the mediocre methanol selectivity over the supported powder Cu/ZnO-based catalysts. Regarding the direct contact Cu-ZnO interface, it presents higher methanol selectivity but with poorer activity, probably due to the lack of highly active H species and the accumulation of ZnOH, behaving like oxide catalysts. The further improvement of methanol selectivity over highly active Cu/ZnO-based catalysts is still a challenge due to stringent requirements of advanced surface characterization techniques and the lack of fine regulated material synthesis technologies. The development of other non-Cu/ZnO-based catalysts should be a promising option to obtain highly efficient catalysts for CO₂ hydrogenation to methanol. More importantly, this work provides an effective strategy to investigate the catalytic behaviors over different reactive interfaces on supported powder model catalysts in the actual reaction conditions, eliminating the pressure gap and material gap.

CRediT authorship contribution statement

Ziyang Chen: Data curation, Formal analysis, Investigation, Validation, Writing – original draft, Writing – review & editing. **Jinjun Wen:** Data curation, Investigation, Validation. **Yu Zeng:** Investigation. **Mengyuan Li:** Validation. **Yukun Tian:** Investigation. **Fan Yang:** Validation. **Molly Meng-Jung Li:** Writing – review & editing. **Peirong Chen:** Writing – review & editing. **Haomin Huang:** Writing – review & editing. **Daiqi Ye:** Funding acquisition, Writing – review & editing. **Limin Chen:** Funding acquisition, Project administration, Writing – review & editing.

Declaration of Competing Interest

The authors declare that they have no known competing financial interests or personal relationships that could have appeared to influence the work reported in this paper.

Data Availability

Data will be made available on request.

Acknowledgements

This work was financially supported by the National Natural Science Foundation of China [No. 21976059, 22276060, 51878292]; Guangdong Basic and Applied Basic Research Foundation (2019A1515011849) and China Scholarship Council Scholarship (CSC No. 201906155006).

Appendix A. Supporting information

Supplementary data associated with this article can be found in the online version at [doi:10.1016/j.apcatb.2023.123192](https://doi.org/10.1016/j.apcatb.2023.123192).

References

- [1] M. Zabilskiy, V.L. Sushkevich, M.A. Newton, J.A. van Bokhoven, Copper-zinc alloy-free synthesis of methanol from carbon dioxide over Cu/ZnO/faujasite, *ACS Catal.* 10 (2020) 14240–14244.
- [2] M. Zabilskiy, V.L. Sushkevich, D. Palagin, M.A. Newton, F. Krumeich, J.A. van Bokhoven, The unique interplay between copper and zinc during catalytic carbon dioxide hydrogenation to methanol, *Nat. Commun.* 11 (2020) 2409.
- [3] N.J. Divins, D. Kordus, J. Timoshenko, I. Sinev, I. Zegkinoglou, A. Bergmann, S. W. Chee, S. Widrina, O. Karslioglu, H. Mistry, M. Lopez Luna, J.Q. Zhong, A. S. Hoffman, A. Boubnov, J.A. Boscoboinik, M. Heggen, R.E. Dunin-Borkowski, S.

R. Bare, B.R. Cuenya, Operando high-pressure investigation of size-controlled CuZn catalysts for the methanol synthesis reaction, *Nat. Commun.* 12 (2021) 1435.

[4] A. Beck, M. Zabilskiy, M.A. Newton, O. Safonova, M.G. Willinger, J.A. van Bokhoven, Following the structure of copper-zinc-alumina across the pressure gap in carbon dioxide hydrogenation, *nature, Catalysis* 4 (2021) 488–497.

[5] S.M. Fehr, K. Nguyen, C. Njel, I. Krossing, Enhancement of methanol synthesis by oxidative fluorination of Cu/ZnO catalysts—insights from surface analyses, *ACS Catal.* 11 (2021) 13223–13235.

[6] A.O. Elnabawy, R. Schimmenti, A. Cao, J.K. Nørskov, Why ZnO is the support for Cu in methanol synthesis? a systematic study of the strong metal support interactions, *ACS Sustain. Chem. Eng.* 10 (2022) 1722–1730.

[7] Y. Shao, M. Kosari, S. Xi, H.C. Zeng, Single solid precursor-derived three-dimensional nanowire networks of cuzn-silicate for Co₂ hydrogenation to methanol, *ACS Catal.* 12 (2022) 5750–5765.

[8] R. Dalebout, L. Barberis, G. Totarella, S.J. Turner, C. La Fontaine, F.M.F. de Groot, X. Carrier, A.M.J. van der Eerden, F. Meirer, P.E. de Jongh, Insight into the nature of the ZnO_x promoter during methanol synthesis, *ACS Catal.* 12 (2022) 6628–6639.

[9] Y. Shi, P. Kang, C. Shang, Z. Liu, Methanol synthesis from CO₂/CO mixture on Cu/Zn catalysts from microkinetics-guided machine learning pathway search, *J. Am. Chem. Soc.* 144 (2022) 13401–13414.

[10] X.Y. Liu, J. Luo, H.W. Wang, L. Huang, S.S. Wang, S. Li, Z.H. Sun, F.F. Sun, Z. Jiang, S.Q. Wei, W.X. Li, J.L. Lu, In situ spectroscopic characterization and theoretical calculations identify partially reduced ZnO_{1-x}/Cu interfaces for methanol synthesis from CO₂, *Angew. Chem. Int. Ed.* 61 (2022).

[11] P. Amann, B. Klotzer, D. Degerman, N. Kopfle, T. Gotsch, P. Lomker, C. Rameshan, K. Ploner, D. Bikaljevic, H.Y. Wang, M. Soldemo, M. Shipilin, C.M. Goodwin, J. Gladh, J.H. Stenlid, M. Borner, C. Schlueter, A. Nilsson, The state of zinc in methanol synthesis over a Zn/ZnO/Cu(211) model catalyst, *Science* 376 (2022) 603–608.

[12] H. Zhao, R. Yu, S. Ma, K. Xu, Y. Chen, K. Jiang, Y. Fang, C. Zhu, X. Liu, Y. Tang, L. Wu, Y. Wu, Q. Jiang, P. He, Z. Liu, L. Tan, The role of Cu₁O₃ species in single-atom Cu/ZrO₂ catalyst for CO₂ hydrogenation, *Nat. Catal.* 5 (2022) 818–831.

[13] X. Liu, J. Luo, H. Wang, L. Huang, S. Wang, S. Li, Z. Sun, F. Sun, Z. Jiang, S. Wei, W. X. Li, J. Lu, In situ spectroscopic characterization and theoretical calculations identify partially reduced ZnO_{1-x}/Cu interfaces for methanol synthesis from CO₂, *Angew. Chem. Int. Ed.* 61 (2022).

[14] S. Jin, Z. Zhang, D. Li, Y. Wang, C. Lian, M. Zhu, Alcohol-Induced strong metal-support interactions in a supported copper/ZnO catalyst, *Angew. Chem. Int. Ed.* (2023), e202301563.

[15] J.E.N. Swallow, E.S. Jones, A.R. Head, J.S. Gibson, R.B. David, M.W. Fraser, M. A. van Spronsen, S. Xu, G. Held, B. Eren, R.S. Weatherup, Revealing the role of CO during CO₂ hydrogenation on Cu surfaces with in situ soft X-Ray spectroscopy, *J. Am. Chem. Soc.* 145 (2023) 6730–6740.

[16] W. Tu, P. Ren, Y. Li, Y. Yang, Y. Tian, Z. Zhang, M. Zhu, Y.C. Chin, J. Gong, Y. Han, Gas-dependent active sites on Cu/ZnO Clusters for CH₃OH Synthesis, *J. Am. Chem. Soc.* 145 (2023) 8751–8756.

[17] M. Yang, J. Yu, A. Zimina, B.B. Sarma, L. Pandit, J.D. Grunwaldt, L. Zhang, H. Xu, J. Sun, Probing the nature of zinc in copper-zinc-zirconium catalysts by operando spectroscopies for CO₂ hydrogenation to methanol, *Angew. Chem. Int. Ed.* 62 (2023).

[18] R. van den Berg, G. Prieto, G. Korpershoek, L.I. van der Wal, A.J. van Bunningen, S. Læggård-Jørgensen, P.E. de Jongh, K.P. de Jong, Structure sensitivity of Cu and CuZn catalysts relevant to industrial methanol synthesis, *Nat. Commun.* 7 (2016) 13057.

[19] S. Kattel, P.J. Ramirez, J.G. Chen, J.A. Rodriguez, P. Liu, Active sites for CO₂ hydrogenation to methanol on Cu/ZnO catalysts, *Science* 355 (2017) 1296–1299.

[20] C. Tisseraud, C. Comminges, S. Pronier, Y. Pouilloux, A. Le, Valant, The Cu-ZnO synergy in methanol synthesis part 3: Impact of the composition of a selective Cu@ZnO core-shell catalyst on methanol rate explained by experimental studies and a concentric spheres model, *J. Catal.* 343 (2016) 106–114.

[21] A. Gotti, R. Prins, Basic metal oxides as cocatalysts for Cu/SiO₂ catalysts in the conversion of synthesis gas to methanol, *J. Catal.* 178 (1998) 511–519.

[22] T. Fujitani, J. Nakamura, The chemical modification seen in the Cu/ZnO methanol synthesis catalysts, *Appl. Catal. A-Gen.* 191 (2000) 111–129.

[23] S. Kuld, C. Conradsen, P.G. Moses, I. Chorkendorff, J. Sehested, Quantification of zinc atoms in a surface alloy on copper in an industrial-type methanol synthesis catalyst, *Angew. Chem. Int. Ed.* 53 (2014) 5941–5945.

[24] S. Kuld, M. Thorhauge, H. Falsig, C.F. Elkjaer, S. Helveg, I. Chorkendorff, J. Sehested, Quantifying the promotion of Cu catalysts by ZnO for methanol synthesis, *Science* 352 (2016) 969–974.

[25] M. Behrens, F. Studt, I. Kasatkina, S. Kühn, M. Hävecker, F. Abild-Pedersen, S. Zander, F. Girsigdes, P. Kurr, B. Kniep, M. Tovar, R.W. Fischer, J.K. Nørskov, R. Schlögl, The active site of methanol synthesis over Cu/ZnO/Al₂O₃ industrial catalysts, *Science* 336 (2012) 893–897.

[26] T. Lunkenstein, J. Schumann, M. Behrens, R. Schloegl, M.G. Willinger, Formation of a ZnO overlayer in industrial Cu/ZnO/Al₂O₃ catalysts induced by strong metal-support interactions, *Angew. Chem. Int. Ed.* 54 (2015) 4544–4548.

[27] T. Lunkenstein, F. Girsigdes, T. Kandemir, N. Thomas, M. Behrens, R. Schloegl, E. Frei, Bridging the time gap: a copper/zinc oxide/aluminum oxide catalyst for methanol synthesis studied under industrially relevant conditions and time scales, *Angew. Chem. Int. Ed.* 55 (2016) 12708–12712.

[28] J. Nakamura, I. Nakamura, T. Uchijima, Y. Kanai, T. Watanabe, M. Saito, T. Fujitani, A surface science investigation of methanol synthesis over a Zn-deposited polycrystalline Cu surface, *J. Catal.* 160 (1996) 65–75.

[29] S.D. Senanayake, P.J. Ramirez, I. Waluyo, S. Kundu, K. Mudiyanselage, Z. Liu, Z. Liu, S. Axnanda, D.J. Stacchiola, J. Evans, J.A. Rodriguez, Hydrogenation of CO₂ to methanol on CeO_x/Cu(111) and ZnO/Cu(111) catalysts: role of the metal-oxide interface and importance of Ce³⁺ sites, *J. Phys. Chem. C* 120 (2016) 1778–1784.

[30] B. Liu, I.M.N. Groot, Q. Pan, S. Shailchutdinov, H. Freund, Ultrathin Zn and ZnO Films on Cu(111) as model catalysts, *Appl. Catal. A-Gen.* 548 (2017) 16–23.

[31] R.M. Palomino, P.J. Ramirez, Z. Liu, R. Hamlyn, I. Waluyo, M. Mahapatra, I. Orozco, A. Hunt, J.P. Simonovis, S.D. Senanayake, J.A. Rodriguez, Hydrogenation of CO₂ on ZnO/Cu(100) and ZnO/Cu(111) catalysts: role of copper structure and metal-oxide interface in methanol synthesis, *J. Phys. Chem. B* 122 (2018) 794–800.

[32] T. Reichenbach, K. Mondal, M. Jaeger, T. Vent-Schmidt, D. Himmel, V. Dybbert, A. Bruix, I. Krossing, M. Walter, M. Moseler, Ab initio study of CO₂ hydrogenation mechanisms on inverse ZnO/Cu catalysts, *J. Catal.* 360 (2018) 168–174.

[33] W.S.K.J. Lee, Thermodynamic investigation of methanol and dimethyl ether synthesis from CO₂ hydrogenation, *Korean J. Chem. Eng.* 2 (2000) 210–216.

[34] L. Martinez-Suarez, J. Frenzel, D. Marx, B. Meyer, Tuning the reactivity of a Cu/ZnO nanocatalyst via gas phase pressure, *Phys. Rev. Lett.* 110 (2013) 86108.

[35] S. Ren, X. Fan, Z. Shang, W.R. Shoemaker, L. Ma, T. Wu, S. Li, N.B. Klinghoffer, M. Yu, X. Liang, Enhanced catalytic performance of Zr Modified CuO/ZnO/Al₂O₃ catalyst for methanol and DME synthesis via CO₂, *Hydrog., J. CO₂ Util.* 36 (2020) 82–95.

[36] A. Müller, A. Comas-Vives, C. Copéret, Shape and surface morphology of copper nanoparticles under CO₂ hydrogenation conditions from first, *Princ., J. Phys. Chem. C* 125 (2021) 396–409.

[37] B. Liang, J. Ma, X. Su, C. Yang, H. Duan, H. Zhou, S. Deng, L. Li, Y. Huang, Investigation on deactivation of Cu/ZnO/Al₂O₃ catalyst for CO₂ hydrogenation to methanol, *Ind. Eng. Chem. Res* 58 (2019) 9030–9037.

[38] X. Sun, F. Sun, S. Gu, J. Chen, X. Du, J. Wang, Y. Huang, Z. Jiang, Local structural evolutions of CuO/ZnO/Al₂O₃ catalyst for methanol synthesis under operando conditions studied by in situ quick X-ray absorption spectroscopy, *Nucl. Sci. Techn.* 28 (2017) 21.

[39] C. Huang, J. Wen, Y. Sun, M. Zhang, Y. Bao, Y. Zhang, L. Liang, M. Fu, J. Wu, D. Ye, L. Chen, CO₂ hydrogenation to methanol over Cu/ZnO plate model catalyst: effects of reducing gas induced Cu nanoparticle morphology, *Chem. Eng. J.* 374 (2019) 221–230.

[40] Y. Sun, C. Huang, L. Chen, Y. Zhang, M. Fu, J. Wu, D. Ye, Active site structure study of Cu/Plate ZnO model catalysts for CO₂ hydrogenation to methanol under the real reaction conditions, *J. CO₂ Util.* 37 (2020) 55–64.

[41] G.R. Li, T. Hu, G.L. Pan, T.Y. Yan, X.P. Gao, H.Y. Zhu, Morphology-function relationship of ZnO: polar planes, oxygen vacancies, and activity, *J. Phys. Chem. C* 112 (2008) 11859–11864.

[42] M. Ashokkumar, S. Muthukumaran, Structural, morphological and spectroscopic investigation of Mn doped Zn_{0.96}Cu_{0.04}O nanoparticles, *J. Mater. Sci.: Mater. Electron.* 26 (2015) 1225–1233.

[43] D. Li, Y.H. Leung, A.B. Djurisic, Z.T. Liu, M.H. Xie, S.L. Shi, S.J. Xu, W.K. Chan, Different origins of visible luminescence in ZnO nanostructures fabricated by the chemical and evaporation methods, *Appl. Phys. Lett.* 85 (2004) 1601–1603.

[44] A.B. Djurisic, W. Choy, V. Roy, Y.H. Leung, C.Y. Kwong, K.W. Cheah, T. Rao, W. K. Chan, H.T. Lui, C. Surya, Photoluminescence and electron paramagnetic resonance of ZnO tetrapod structure, *Adv. Funct. Mater.* 14 (2004) 856–864.

[45] H. Alnoor, A. Savoyant, X. Liu, G. Pozina, M. Willander, O. Nur, An effective low-temperature solution synthesis of Co-Doped [0001]-oriented ZnO nanorods, *J. Appl. Phys.* 121 (2017), 215102.

[46] H.P. He, J.G. Guo, X.D. Xie, J.L. Peng, Location and migration of cations in Cu²⁺-adsorbed montmorillonite, *Environ. Int.* 26 (2001) 347–352.

[47] G. Li, N.M. Dimitrijevic, L. Chen, T. Rajh, K.A. Gray, Role of surface/interfacial Cu²⁺ sites in the photocatalytic activity of coupled CuO-TiO₂ nanocomposites, *J. Phys. Chem. C* 112 (2008) 19040–19044.

[48] J. Xue, X. Wang, G. Qi, J. Wang, M. Shen, W. Li, Characterization of copper species over Cu/SAPO-34 in selective catalytic reduction of NO_x with ammonia: relationships between active Cu Sites and de-NO_x performance at low temperature, *J. Catal.* 297 (2013) 56–64.

[49] X. Yang, H. Chen, Q. Meng, H. Zheng, Y. Zhu, Y.W. Li, Insights into influence of nanoparticle size and metal-support interactions of Cu/ZnO catalysts on activity for furfural hydrogenation, *Catal. Sci. Technol.* 7 (2017) 5625–5634.

[50] N.Y. Topsøe, H. Topsøe, FTIR studies of Dynamic Surface Structural Changes in Cu-Based Methanol Synthesis, *Catal., J. Mol. Catal. A: Chem.* 141 (1999) 95–105.

[51] S. Kannan, T. Venkov, K. Hadjivanov, H. Knozinger, Fourier transform infrared study of low-temperature CO Adsorption on CuMgAl-hydrotalcite, *Langmuir* 20 (2004) 730–736.

[52] M.C. Biesinger, L. Lau, A.R. Gerson, R. Smart, Resolving surface chemical states in XPS analysis of first row transition metals, oxides and hydroxides: Sc, Ti, V, Cu and Zn, *Appl. Surf. Sci.* 257 (2010) 887–898.

[53] K. Klier, V. Chatikavanij, R.G. Herman, G.W. Simmons, Catalytic synthesis of methanol from CO/H₂ IV. The effects of carbon dioxide, *J. Catal.* (1982) 343–360.

[54] J.S. LEE, K.H. LEE, S.Y. LEE, Y.G. KIM, A comparative study of methanol synthesis from CO₂/H₂ and CO/H₂ over a Cu/ZnO/Al₂O₃ catalyst, *J. Catal.* (1993) 414–424.

[55] F.C.F. Marcos, L. Lin, L.E. Betancourt, S.D. Senanayake, J.A. Rodriguez, J.M. Assaf, R. Giudici, E.M. Assaf, Insights into the methanol synthesis mechanism via CO₂ hydrogenation over Cu-ZnO-ZrO₂ catalysts: effects of surfactant/Cu-Zn-Zr Molar Ratio, *J. CO₂ Util.* 41 (2020), 101215.

[56] C. Li, H. Liang, J. Zhao, Q. Feng, J. Bian, Y. Liu, R. Shen, W. Li, G. Wu, G.T. Du, Influence of high-pressure hydrogen treatment on structural and electrical properties of ZnO thin films, *Appl. Surf. Sci.* 256 (2010) 6770–6774.

[57] K. Nishidate, M. Hasegawa, Hydrogen-induced disruption of the ZnO(0001) polar surface, *Phys. Rev. B: Condens. Matter Mater. Phys.* 86 (2012) 35412.

[58] H. Li, K. Karahashi, P. Friederich, K. Fink, M. Fukasawa, A. Hirata, K. Nagahata, T. Tatsumi, W. Wenzel, S. Hamaguchi, Effects of hydrogen ion irradiation on zinc oxide etching, *J. Vac. Sci. Technol. A* 35 (2017) 05C303.

[59] P. Kumar, G.K. Inwati, M.C. Mathpal, S. Ghosh, W.D. Roos, H.C. Swart, Defects induced enhancement of antifungal activities of Zn doped CuO nanostructures, *Appl. Surf. Sci.* 560 (2021), 150026.

[60] Y.Y. Tay, S. Li, C.Q. Sun, P. Chen, Size dependence of Zn 2p 3/2 binding energy in nanocrystalline ZnO, *Appl. Phys. Lett.* 88 (2006), 173118.

[61] C. Temvuttirojn, Y. Poo-arporn, N. Chanlek, C.K. Cheng, C.C. Chong, J. Limtrakul, T. Witoon, Role of calcination temperatures of ZrO₂ support on methanol synthesis from CO₂ hydrogenation at high reaction temperatures over ZnO_x/ZrO₂ catalysts, *Ind. Eng. Chem. Res* 59 (2020) 5525–5535.

[62] G. Ballerini, K. Ogle, M.G. Barthès-Labrousse, The acid-base properties of the surface of native zinc oxide layers: An XPS study of adsorption of 1,2-diaminoethane, *Appl. Surf. Sci.* 253 (2007) 6860–6867.

[63] B. Song, Y. Li, X. Wu, F. Wang, M. Lin, Y. Sun, A. Jia, X. Ning, L. Jin, X. Ke, Z. Yu, G. Yang, W. Hou, W. Ding, X. Gong, L. Peng, Unveiling the surface structure of ZnO nanorods and H₂ activation mechanisms with ¹⁷O NMR spectroscopy, *J. Am. Chem. Soc.* 144 (2022) 23340–23351.

[64] E.D. Batyrev, J.C. van den Heuvel, Modification of the ZnO(0001)-Zn surface under reducing conditions, *Phys. Chem. Chem. Phys.* 13 (2011) 13127–13134.

[65] Y. Liu, J. Liu, S. Liu, J. Li, Z. Gao, Z. Zuo, W. Huang, Reaction mechanisms of methanol synthesis from CO/CO₂ hydrogenation on Cu₂O(111): comparison with Cu(111), *J. CO₂ Util.* 20 (2017) 59–65.

[66] J. Ye, C. Liu, Q. Ge, DFT study of CO₂ adsorption and hydrogenation on the In₂O₃ surface, *J. Phys. Chem. C* 116 (2012) 7817–7825.

[67] A.J. Medford, J. Sehested, J. Rossmeisl, I. Chorkendorff, F. Studt, J.K. Nørskov, P. G. Moses, Thermochemistry and micro-kinetic analysis of methanol synthesis on ZnO (0001), *J. Catal.* 309 (2014) 397–407.

[68] J. Wang, G. Li, Z. Li, C. Tang, Z. Feng, H. An, H. Liu, T. Liu, C. Li, A highly selective and stable ZnO-ZrO₂ solid solution catalyst for CO₂ hydrogenation to methanol, *Sci. Adv.* (2017), e1701290.

[69] Q.L. Tang, W.T. Zou, R.K. Huang, Q. Wang, X.X. Duan, Effect of the components' interface on the synthesis of methanol over Cu/ZnO from CO₂/H₂: a microkinetic analysis based on DFT + U calculations, *Phys. Chem. Chem. Phys.* 17 (2015) 7317–7333.

[70] M. Huš, D. Kopač, N.S. Štefančić, D.L. Jurković, V.D.B.C. Dasireddy, B. Likozar, Unravelling the mechanisms of CO₂ hydrogenation to methanol on Cu-based catalysts using first-principles multiscale modelling and experiments, *Catal. Sci. Technol.* 7 (2017) 5900–5913.